PCCP

RSC Publishing

PAPER

Computer simulations of cluster impacts: effects of the atomic masses of the projectile and target

Cite this: *Phys. Chem. Chem. Phys.*, 2013, **15**, 7621

Oscar A. Restrepo,* Xavier Gonze, Patrick Bertrand and Arnaud Delcorte

Received 24th January 2013,
Accepted 20th February 2013

DOI: 10.1039/c3cp50346a

www.rsc.org/pccp

Cluster secondary ion mass spectrometry is now widely used for the characterization of nanostructures. In order to gain a better understanding of the physics of keV cluster bombardment of surfaces and nanoparticles (NPs), the effects of the atomic masses of the projectile and of the target on the energy deposition and induced sputtering have been studied by means of molecular dynamics simulations. 10 keV C_{60} was used as a model projectile and impacts on both a flat polymer surface and a metal NP were analyzed. In the first case, the mass of the impinging carbon atoms was artificially varied and, in the second case, the mass of the NP atoms was varied. The results can be rationalized on the basis of the different atomic mass ratios of the projectile and target. In general, the emission is at its maximum, when the projectile and target have the same atomic masses. In the case of the supported NP, the emission of the underlying organic material increases as the atomic mass of the NP decreases. However, it is always less than that calculated for the bare organic surface, irrespective of the mass ratio. The results obtained with C_{60} impacts on the flat polymer are also compared to simulations of C_{60} and monoatomic Ga impacts on the NP.

1. Introduction

In the last decade, cluster beams have revolutionized the field of secondary ion mass spectrometry (SIMS), providing much higher sensitivities for the analysis and the possibility to perform depth profiling with retention of the molecular information.[1–3] Energetic clusters are also used in the fabrication process of materials, as dopants in the surface layer or to clean the surfaces.[4,5] In order to ground future developments of the technique in a scientific approach rather than a trial-and-error procedure, it seems important to fully understand the physical parameters that govern the cluster projectile penetration, energy transfer and induced sputtering. Among them, the mass of the projectile atoms and the atomic mass ratio between the projectile and the target are central to explain the effects.[6] To reach this goal, a good method, apt to handle the millions of atoms involved in the cluster–surface interaction event and in which the parameters can be easily varied, is molecular dynamics (MD) simulations.[7]

Recent MD studies[8–13] have indicated that the maximum sputter yield is obtained when the projectile and target atomic masses are equal. However, none of the works discusses this observation in detail. For instance, in the keV energy regime, that fact was verified in the case of C_{60} impinging on graphite, fullerite or other organic substrates,[9,10] where the main components are carbon atoms. It is also valid for heavy clusters like Au_{400} impinging gold.[8,11,14] In these cases, if the attractive interaction energy between the projectile atoms is negligible with respect to the initial kinetic energy per atom, the energy is deposited in a spherical region. A large emission yield is observed and a spherical crater is formed depending on the target density.

A more complex case occurs for nanoparticles (NPs) supported on an organic surface or embedded in an organic matrix, as they are often manufactured by the industry of nanotechnologies. When a NP-containing organic surface is bombarded with keV projectiles, the energy transfer to the NPs will govern their fragmentation and emission. In a similar manner, the sputtering of the organic matrix will also depend on the fragmentation and efficient transfer of the energy of the targeted NPs that are in the projectile trajectory.[15–17] Direct impacts on the NPs will create smaller clusters and free atoms that redistribute the energy in the surface in a specific way. They also stop the projectile and sputter in a different manner to the matrix (preferential sputtering), sometimes producing undesired effects on the analysis[18,19] or the molecular depth profiling. A better understanding of these effects and how they are influenced by the nature of the NP, in particular its atomic mass, should help the analyst to optimize the parameters of the experiment.

Institute of Condensed Matter and Nanosciences, Université catholique de Louvain, Croix du Sud, 1 bte 3, B-1348 Louvain-la-Neuve, Belgium.
E-mail: ores77@gmail.com, arnaud.delcorte@uclouvain.be

In this study, we tackle the effect of mass on cluster-induced sputtering with two model systems mimicking important classes of materials. The first one is a simple polymeric solid and in that case, the effect of mass is investigated by artificially varying the atomic mass of the impinging C_{60} cluster in the range 14–197 amu, keeping all other parameters constant. The second one is a metal NP adsorbed on the same polymer substrate, and with this system, the atomic mass of the NP is varied, in the range 1–197 amu. The investigation of this system also has implications in metal-assisted SIMS.[18,19] In comparison with previously published studies, the novelty of our approach resides in the gradual variation of the atomic mass within a wide range of values while all the other parameters are kept constant. In this manner, more detailed trends are obtained and interference with the effect of other physical properties (structure, cohesive energy) is deliberately avoided. In addition, the total kinetic energy and the energy per atom in the projectile, often the primary defining factors in cluster bombardment of solids, are kept constant through all our simulations. The analysis of the results focuses on the dependence of sputtering on the mass, the projectile penetration and energy transfer to the surface and the NP fragmentation.

2. Computational method

In order to describe the time-evolution of the system of interest, classical molecular dynamics (MD) simulations were implemented using the SPUT code.[20] The sample construction and deposition of the gold NPs were already discussed in previous works[14–16,21] and the detailed explanation of the MD simulation methodology can be found elsewhere.[22,23] The sample consists of a box with either 2400 chains or 4800 chains (used when projectile atomic mass is varied) of polyethylene (PE), each chain being formed of 200 individual CH_2 coarse grain elements, and the dimensions of the system are $300 \times 250 \times 150$ Å^3 (or $300 \times 250 \times 300$ Å^3). The surface was coated with 13 386 Au atoms forming NPs of 20–30 Å of diameter. Therefore, the system was made of a total of 493 386 elements for the first case and 1 056 386 elements for the second case. The interaction potentials used were the MD/MC-CEM potential for Au–Au,[24] Lennard Jones potential functions for Au–PE and PE–PE intermolecular interactions, the AIREBO potential for the C–C interactions of the C_{60} projectile[25] and Morse potential functions for the intramolecular interactions in PE. Additional details about the potential parameters can be found in ref. 26. For visualization, the VMD program was used.[27]

The selected projectiles were C_{60} and Ga aimed at the surface with a normal incidence. To understand the effect of changing the atomic masses of the target and the projectile, two sets of MD simulations were run, up to 30 ps. In the first set of simulations, C_{60} impinging on bare PE, the atomic mass of the projectile was artificially varied. In the second set, where C_{60} and Ga impinge on a supported Au-NP, it is the atomic mass of the gold that was changed. The chosen atomic mass values were 1, 12, 69, 98, 138 and 197 amu, which were equivalent to the masses of Au/197 → H, Au/16 → C, Au/3 → Ga, Au/2 → $7CH_2$, 2Au/3 → 2Ga, and Au itself. The other parameters of the system were kept constant. Because of its polyatomic nature, it is known that C_{60} exhibits only small variations of sputter yield as a function of the impact point,[7] so only one (first system) and three impacts (second system) per value of mass were computed. On the other hand, atomic projectiles such as Ga are known to induce large sputtering fluctuations[7] and a larger number of impacts should in principle be calculated. However, due to the computational expense, only four impacts around the center of the NP were computed in this study. For all the simulations, the impact energy was set to 10 keV. This value fulfills the condition that the projectile energy per atom must be higher than the corresponding interaction energies, and guarantees the full fragmentation of C_{60}.[9] It also ensures that the total kinetic energy and the energy per atom are the same for all the considered calculations. For the relaxation and the bombardment, rigid boundaries of 0.5 nm and stochastic forces at 4 K over a region of 1.5 nm were implemented over all the sides, except the bombarded one, using the Langevin equation, to provide a heat bath (during the relaxation) and to absorb the generated pressure waves (during the impact).[28]

3. Results and discussion

3.1. Changing the atomic mass of C_{60}

In the first set of simulations, 10 keV impacts on bare PE were calculated, changing the atomic mass of the C_{60} from 14 to 197 amu. In this case the depth of the simulation box was 300 Å. To obtain an exact match in projectile–target atomic masses, the carbon mass was replaced by the mass of a CG PE unit, equal to 14 amu. The results are given in the four plots of Fig. 1. In the top graphs of Fig. 1, the sputtered masses and their corresponding kinetic energies have been gathered at 3 ps and 20 ps. Although 3 ps is not sufficient to cover the entire emission process, the results obtained at 20 ps show that the PE emission *vs.* atomic mass keeps almost the same functional form in time. In addition, the comparison shows that, of the total quantity of ejected fragments after 20 ps, those fragments that leave the surface before 3 ps transport ~95% of the kinetic energy, and they have only ~30% of the total sputtered mass. In terms of the mass effect, Fig. 1a and b shows that the maximum emission is obtained when the atomic masses match. A reduction of the sputtered mass by more than one order of magnitude is predicted when the projectile atomic mass increases from 14 to 197 amu.

The sputtering results are correlated to the energy transfer in the surface region. Fig. 1c shows the comparison of the energy transfer to the top 3 nm and 5 nm of PE as a function of time, for each value of atomic mass. ~65% of the projectile energy is transferred in the first 120 fs into the top 3 nm layers when the masses are equal. Similar plots for the top 5 nm slab show that the peak maximum increases significantly in all cases except when the atomic mass of the projectile is 14 (as compared to the corresponding peak on the "top 3 nm layer" graph in Fig. 1c). Thus, most of the energy is deposited into the top 3 nm when atomic masses match. The fraction of energy lost by the projectile as it changes its position in space, over the first 1.5 ps, is shown in Fig. 1d (the *t*-axis is scaled by the initial velocity). The differences between the slopes in the linear region are clear. When the projectile and target atomic masses match, the energy

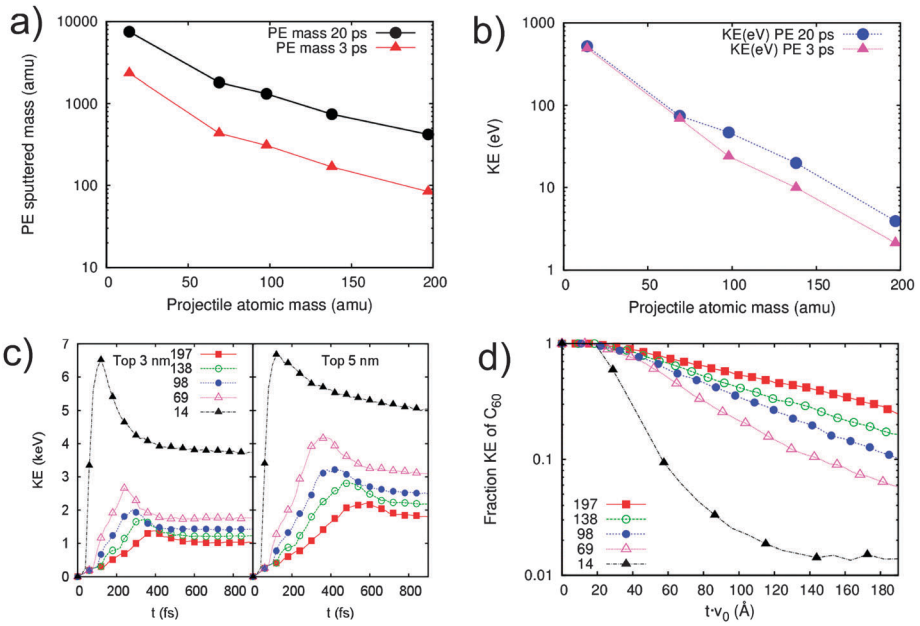

Fig. 1 Top: (a) comparison of the total sputter PE mass and (b) its kinetic energy (KE) as a function of the C_{60} atomic mass at times of 3 and 20 ps. Bottom: (c) comparison of the KE transferred from C_{60} to the top 3 nm and 5 nm of the PE surface. (d) Fraction of kinetic energy retained by the projectile as it changes its position in the space, for the first 1.5 ps.

is fully transferred to the sample surface, while it diffuses over a much larger depth for greater masses. Furthermore, the projectile loses more than ~95% of its energy in the first 200 fs.

In order to establish a more detailed view of the energy transfer from the projectile to the sample, an additional analysis is provided in Fig. 2 for 3 representative cases (atomic mass values equal to PE, Ga and Au). For this purpose, the simulation cell was sliced in horizontal slabs of 3 Å each. Then, the evolution of the kinetic energy in each slab was monitored as a function of time for the different trajectories. These pictures show that, when the atomic mass is increased, the energy tends to remain longer in the projectile and it is transferred to a much greater depth. In the first few femtoseconds, when the transfer of energy is exponential (see the semi logarithmic plot in Fig. 1d), the cluster impact generates an energy wave in the substrate, with an intensity that is proportional to the impact energy. Afterwards, the wave starts to be damped because no more energy is transferred from the projectile. The lighter rays developing above the sample surface (negative Z values) indicate the sputtering of PE fragments. Their intensity is inversely proportional to the C_{60} atomic mass.

The top panel of Fig. 3 compares the C_{60} projectiles fragmentation and dispersion when they impact on PE, with the same atomic mass values as Fig. 2. The comparison is made at three different times: 200, 500 and 1000 fs and using different colors for each mass value; this to differentiate better the mass effects. These pictures show that the maximum dispersion occurs when the projectile and target have the same atomic masses. The bottom frames also indicate the PE damage and crater formation after 1500 fs. Those pictures corroborate and help to explain the results shown in Fig. 1 and 2. When the projectile is

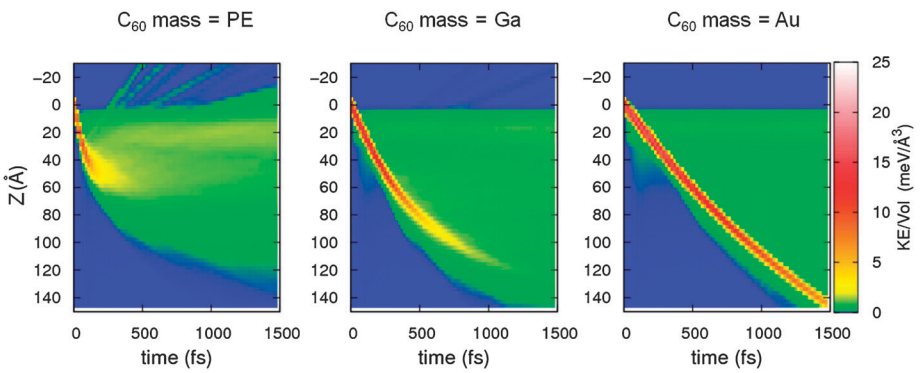

Fig. 2 Evolution of the kinetic energy per layer volume (KE/Vol) in the sample for 10 keV C_{60} impacts on PE as a function of the projectile atomic mass: C_{60} → PE, C_{60} → Ga and C_{60} → Au. At 3000 fs, the interval between frames is 20 fs. The KE/Vol in each horizontal slab of 3 Å is color-coded from blue to white (color scale on the right).

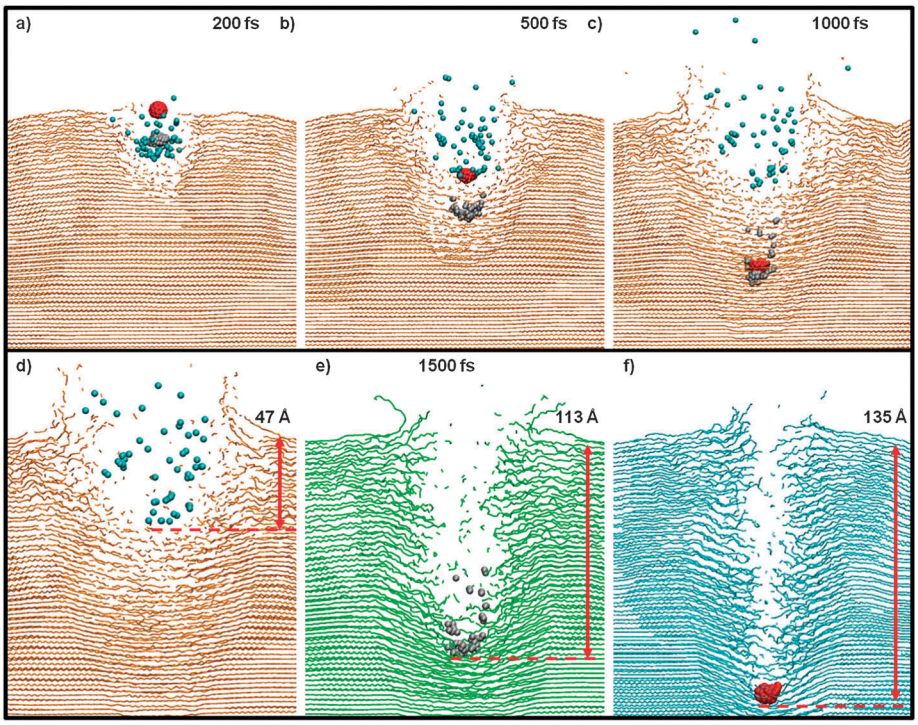

Fig. 3 Top: comparison of the projectile fragmentation when the C_{60} atomic mass is equivalent to the mass of PE (blue), Ga (gray) and Au (red), at three different times. Only the damage by the blue projectile is shown (coffee color). Bottom: crater shapes as a function of the atomic mass at 1500 fs.

heavier than the target, it implants deeper and its atoms are not strongly dispersed. Hence, the target bonds are only broken in the initial projectile direction, in a narrow vertical track. However, when the atomic masses of the projectile and target match, the crater becomes spherical, due to a broad dispersion of the projectile atoms. Similar conclusions on the effect of the mass ratio were drawn by *e.g.* Urbassek *et al.* for impacts of C_{60} on a series of surfaces (carbon, argon, gold) but, in that case, the substrate structures and cohesive energies were also markedly different.[9]

The ranges of the center of mass (R_{CM}) and of the deepest implanted atom (R_{max}) are plotted in Fig. 4 as a function of the projectile momentum. The range increases linearly with the atomic mass, in correlation with the decrease of the mass of ejected fragments (Fig. 1). The linearity of the range *vs.* momentum relationship is in agreement with the results shown for experiments and simulations with cobalt cluster bombardment of graphite made by Popok and co-workers.[29] It should be noted that these authors divided the momentum by the projected surface area of the projectile on the surface, but in our case, this area is constant, as is the projectile size.

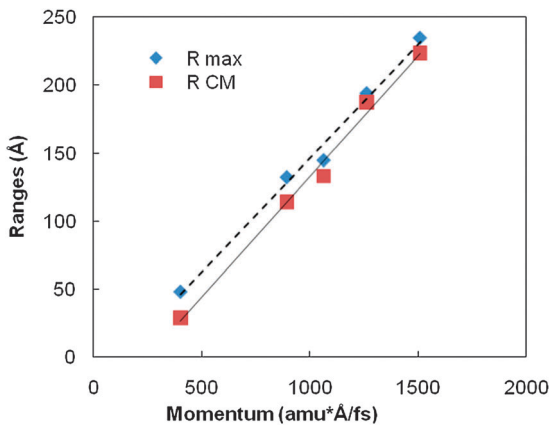

Fig. 4 Ranges of the center of mass (R_{CM}) and of the deepest implanted atom (R_{max}) in PE for the impacts of 10 keV C_{60} clusters with modified atomic masses, plotted as a function of the projectile momentum.

3.2. Changing the atomic mass of the NPs

For these simulations, we used the smaller system, where the PE surface was covered by Au-NPs. The atomic mass of the NPs was replaced by the values mentioned above, *i.e.* 1, 12, 69, 98, 138 and 197 amu. For each atomic mass, three impacts were calculated with C_{60} and four with Ga, one at the center of the Au_{555} NP and the others at 2 Å on each side, to obtain some information on the stochastic variation of the NP fragmentation and sputtering. After 30 ps, the ejected mass and yields of PE and Au fragments were gathered and analyzed (Fig. 5). It should be noted that, for the considered metal–organic system, some late events might still happen after 30 ps, such as desorption of massive intact NPs at large distances from the impact. Therefore, caution should be used in the discussion of the gold sputtered mass and only the fragments of the central NP are considered in Fig. 5. An additional set of five simulations with C_{60} impinging on PE at different impact points were also calculated to compare with the impacts on the NP. These results are represented by the point with the error bar that shows the corresponding interval of

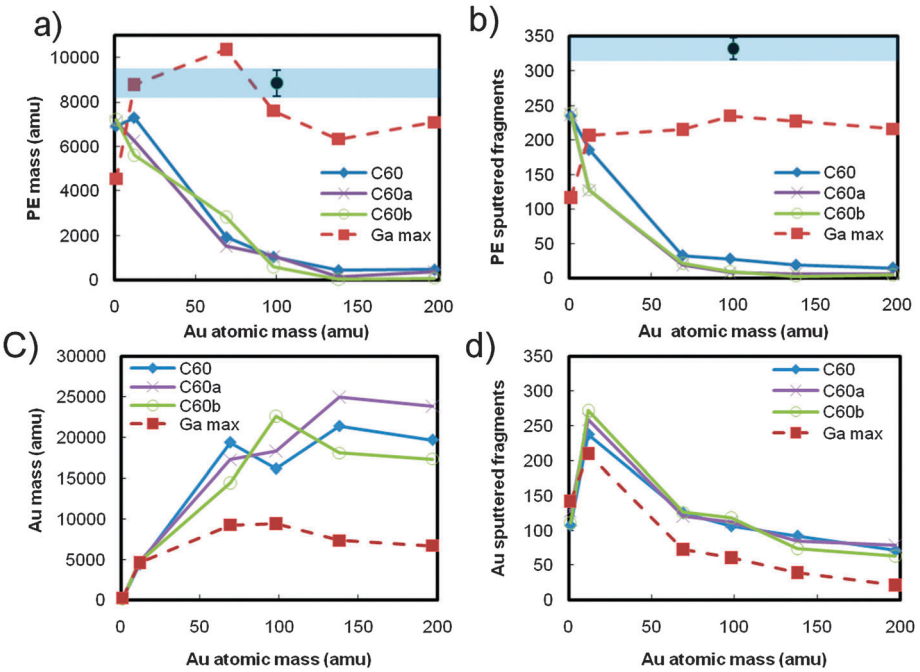

Fig. 5 Sputtered masses (a, c) and numbers of fragments (b, d) as a function the NP atomic mass, after 30 ps, for impacts on the NP. For (a) and (b), the data are compared with the interval of emission of the C_{60} impacts over a bare area of the PE surface (blue band). The dashed red line corresponds to the maximum yield of Ga (from a set of four impacts).

emission (blue band in Fig. 5a and b). First, as indicated by the green, blue and purple lines, it is confirmed that the influence of the exact impact point on the NP is secondary in the case of C_{60}.

The results of the C_{60} impacts on the NP show that the emission yield of polymer decreases as the atomic mass of the NP increases (Fig. 5b), and that the number of sputtered Au fragments decreases as the atomic mass of the NP increases beyond 12 amu (Fig. 5d). This can be explained as follows. As the NP atomic mass increases, the inertia of the gold and the reflection of the carbon atoms become more important and the energy transfer to the target in each collision is reduced. Note that, although the PE sputtered mass increases as the mass of the NP decreases, the maximum remains lower than the value observed for the C_{60} impacts on bare PE. This can be explained by the energy wasted to break the bonds of the NP. Concerning the Au-NP, the maximum number of fragments is predicted for a mass of 12 amu, *i.e.*, when mass matching occurs. This corresponds to the maximum energy transfer $[4M_1M_2/(M_1 + M_2)^2]$ in binary collisions (BC) involving the considered partners. The similarity of the plot of maximum energy transfer in BC (not shown) to the plots of the sputtered Au cluster yield is striking, suggesting that the interpretation of the sputtered yield can be based on the results of separated atom–atom interactions rather than collective effects in this case, as if every C atom of the projectile was directly backscattered by one Au atom of the target and the NP fragmentation directly proportional to the transferred energy. Finally, Fig. 5c indicates that the reduction of the number of fragments is offset by the increasing atomic mass, such that the total sputtered mass from the NP first increases and then saturates (beyond 100 amu).

For each atomic mass value, the C_{60} yields were compared to each maximum yield obtained over four impacts with Ga (dashed lines in Fig. 5). The Ga maximum yields were considered rather than the averages because, in most of the cases, the Ga projectile channels into the NP and the polymer without producing yield, so that very large fluctuations are observed. However, in some instances (which depend on small variations of the exact impact point), a rather dense cascade is initiated in the polymer, the energy is efficiently transferred to the surface and a maximum emission is produced. Those cases are of interest because they lead to maximum PE yields that are comparable to the sputtering produced by C_{60} on bare PE. Fig. 5a and b indicates that contrary to C_{60} impact on NP, the Ga maximum PE yields are not strongly affected by the atomic mass variation of the NPs. In addition Fig. 5c and d shows that the sputtered Au mass is, in almost all the cases, smaller for Ga than for C_{60}. Those facts indicate that, almost independently of the NPs atomic mass, the energy of the impact is better transferred to the PE than to the NPs using Ga.

As an illustration, for one of the three impacts for C_{60} and one of the four impacts for Ga, Fig. 6 shows a comparison of the total kinetic energy (KE) per atom of the NP as a function of time for each of the atomic mass values of the NP. For all the plots with C_{60} impacts, the KE of the NP reaches a maximum and later decreases as the energy is transferred to the PE. The peak maximum rises as the projectile and the NP atomic masses become close, having a maximum value when the atomic masses match. The intensities of the peak maxima follow the same sequence as the Au sputter yield (Fig. 5d), confirming the suggested proportionality between the total

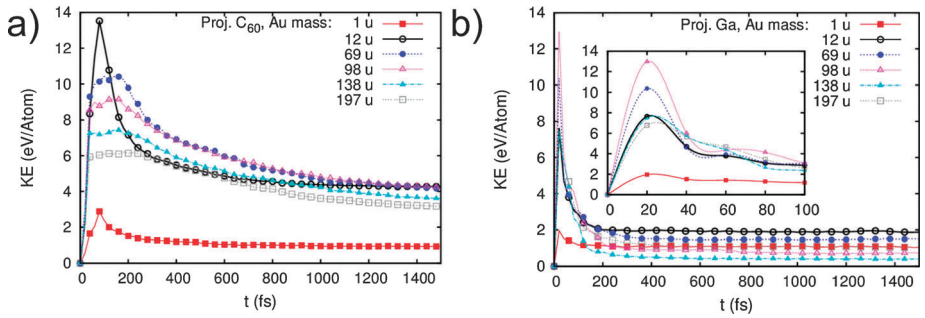

Fig. 6 Time evolution of the average kinetic energy (KE) of the NP upon impacts by C_{60} (a) and Ga (b). The inset of (b) shows a zoom over the peak maxima.

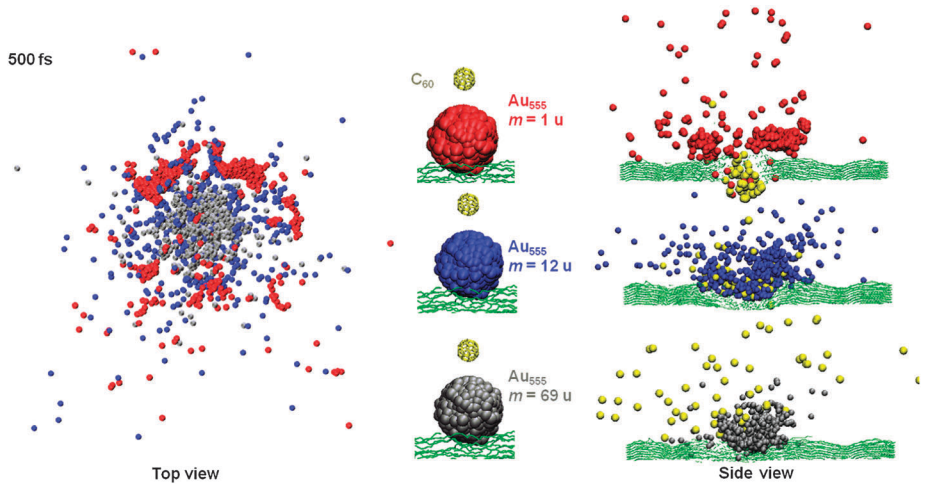

Fig. 7 Comparison of the C_{60}–Au-NP collisions, when the atomic mass of the NP is 1 amu (red), 12 amu (blue) and 69 amu (gray). On the left: top view of the NP fragmentation. On the right: side view of the NP fragmentation and reflection of C_{60} at 500 fs.

energy transferred to the NP and the sputter yield, through the extent of fragmentation. Fig. 6 also shows that the energy transfer from the NP to its environment occurs faster as the atomic mass decreases, as an effect of the target atom inertia. The plots of the other two impacts show similar results, as expected, because of the limited fluctuations of the C_{60}-induced sputtering as a function of the impact point. On the other hand the plots for Ga show a more stochastic nature and a maximum transfer at around 20 fs in all cases (inset of Fig. 6b).

In the collision process of C_{60} with the NP, the manner in which the fragmentation happens depends on the atomic mass of the target atoms. The fragmentation of the target NP is also analyzed using the movies from the simulations in Fig. 7; as before, for each mass value a different color is used. If the NP disintegrates into many fragments that spread laterally with sufficient energy, the energy is more efficiently transferred to the surrounding organic medium and the emission of PE fragments is also enhanced (Fig. 5). This is the case when the projectile and the target NP have the same atomic masses. In Fig. 7, the top view clearly shows the maximized number of fragments (dark blue), while the side view shows their maximum dispersion. When the atomic mass of the target is less than the atomic mass of the projectile, C_{60} goes through it without a significant change of its trajectory. In contrast, when the atomic mass of the target is larger than the atomic mass of C_{60}, the atoms of the projectile are strongly deflected or even backscattered. On the other hand the fragmentation upon Ga impacts is rather stochastic and depends more on the specific impact point than on the atomic mass.

4. Conclusion

The effects of varying the atomic masses of the cluster projectile and the target on the sputtering process have been studied in detail, using a system composed of polyethylene with and without adsorbed metal nanoparticles, bombarded with 10 keV C_{60} and Ga. For impacts on bare PE, it is observed that increasing the atomic mass of C_{60} results in the implantation of the projectile and energy loss into the depth of the target, below the sputtering crater, and in a reduction of the sputter yield. Upon impacts on the Au-NP, the simulations consistently show that the sputter yields of Au and PE decrease rapidly as the atomic mass of the NP increases, with the NP fragmentation being maximum when the atomic masses of the projectile and target NP match. The maximum energy transfer, NP fragmentation and fragment dispersion are also observed when atomic masses match. Atomic masses much smaller for the impinging cluster than the target lead to energy loss *via* reflection of the

projectile constituents. Quite surprisingly, the evolution of the sputter yields is consistent with a simple explanation of energy transfer based on binary collisions. For atomic (Ga) impacts, the results confirm that the NP fragmentation is a random process that depends strongly on the exact impact point.

Acknowledgements

The authors wish to thank Professor B. J. Garrison from Penn State University for the access to her simulation code for MD simulations. This work and OR are supported by the French Community of Belgium *via* the Concerted Research Action programme (ARC NANHYMO: convention 07/12-003) and by the European Community under the FP7 project 3D-Nano-chemiscope (Grant agreement: CP-TP 200613-2). AD is a Senior Research Associate of the Belgian Fonds National pour la Recherche Scientifique (FNRS). Computational resources have been provided by the supercomputing facilities of the Université catholique de Louvain (CISM/UCL).

References

1 C. Mahoney, *Mass Spectrom. Rev.*, 2010, **29**, 247–293.
2 N. Davies, D. E. Weibel, P. Blenkinsopp, N. Lockyer, R. Hill and J. C. Vickerman, *Appl. Surf. Sci.*, 2003, **203–204**, 223–227.
3 N. Winograd, *Rev. Anal. Chem.*, 2005, **77**, 143A–149A.
4 D. S. McPhail, *J. Mater. Sci.*, 2006, **41**, 873–903.
5 I. Yamada, J. Matsuo, N. Toyoda and A. Kirkpatrick, *Mater. Sci. Eng.*, 2001, **34**(6), 231–295.
6 A. Delcorte, O. A. Restrepo, B. Czerwinski and B. J. Garrison, *Surf. Interface Anal.*, 2013, **45**, 9–13.
7 B. J. Garrison and Z. Postawa, *Mass Spectrom. Rev.*, 2008, **27**, 289–315.
8 C. Anders and H. Urbassek, *Nucl. Instrum. Methods Phys. Res., Sect. B*, 2005, **228**, 57–63.
9 C. Anders, H. Kirihata, Y. Yamaguchi and H. Urbassek, *Nucl. Instrum. Methods Phys. Res., Sect. B*, 2007, **255**, 247–252.
10 A. Delcorte and B. J. Garrison, *J. Phys. Chem. C*, 2007, **111**, 15312–15324.
11 S. Zimmermann and H. Urbassek, *Int. J. Mass Spectrom.*, 2008, **272**, 91–97.
12 C. Anders, G. Ziegenhain, S. Zimmermann and H. M. Urbassek, *Nucl. Instrum. Methods Phys. Res., Sect. B*, 2009, **267**, 3122–3125.
13 C. Anders and H. M. Urbassek, *Nucl. Instrum. Methods Phys. Res., Sect. B*, 2009, **267**, 3227–3231.
14 O. A. Restrepo and A. Delcorte, *J. Phys. Chem. C*, 2011, **115**, 12751–12759.
15 O. A. Restrepo and A. Delcorte, *Surf. Interface Anal.*, 2011, **43**, 70–73.
16 A. Delcorte, P. Bertrand, B. J. Garrison, K. Hamraoui, T. Mouhib, O. A. Restrepo, C. N. Santos and S. Yunus, *Surf. Interface Anal.*, 2010, **42**, 1380–1386.
17 O. Restrepo, A. Prabhakaran, K. Hamraoui, N. Wehbe, S. Yunus, P. Bertrand and A. Delcorte, *Surf. Interface Anal.*, 2010, **42**, 1030–1034.
18 A. Delcorte, S. Yunus, N. Wehbe, N. Nieuwjaer, C. Poleunis, A. Felten, L. Houssiau, J. J. Pireaux and P. Bertrand, *Anal. Chem.*, 2007, **79**, 3673–3689.
19 N. Wehbe, A. Heile, H. F. Arlinghaus, P. Bertrand and A. Delcorte, *Anal. Chem.*, 2008, **80**, 6235–6244.
20 B. J. Garrison, A. Delcorte and K. Krantzman, *Acc. Chem. Res.*, 2000, **33**, 69–77.
21 O. A. Restrepo, A. Prabhakaran and A. Delcorte, *Nucl. Instrum. Methods Phys. Res., Sect. B*, 2011, **269**, 1595–1599.
22 B. J. Garrison, *Chem. Soc. Rev.*, 1992, **21**, 155–162.
23 B. J. Garrison, in *ToF-SIMS: Surface Analysis by Mass Spectrometry;* ed. J. C. Vickerman, D. Briggs, Surface Spectra, Manchester, U.K., 2001, pp. 223–257.
24 M. S. Stave, D. E. Sanders, T. J. Raeker and A. E. DePristo, *J. Chem. Phys.*, 1990, **93**, 4413–4426.
25 S. J. Stuart, A. B. Tutein and J. A. Harrison, *J. Chem. Phys.*, 2000, **112**, 6472–6486.
26 K. Hamraoui and A. Delcorte, *J. Phys. Chem. C*, 2010, **114**, 5458–5467.
27 W. Humphrey, A. Dalke and K. Schulten, VMD – Visual Molecular Dynamics, *J. Mol. Graphics*, 1996, **14**, 33–38, http://www.ks.uiuc.edu/Research/vmd/.
28 Z. Postawa, B. Czerwinski, M. Szewczyk, E. J. Smiley, N. Winograd and B. J. Garrison, *Anal. Chem.*, 2003, **75**, 4402.
29 V. Popok, J. Samela, K. Nordlund and E. Campbell, *Phys. Rev. B: Solid State*, 2010, **82**, 1–4.